Langmuir

Article

pubs.acs.org/Langmuir

Ultralow Adhesion and Friction of Fluoro-Hydro Alkyne-Derived Self-Assembled Monolayers on H-Terminated Si(111)

Sidharam P. Pujari,[†] Evan Spruijt,[‡] Martien A. Cohen Stuart,[‡] Cees J. M. van Rijn,[†] Jos M. J. Paulusse,[†] and Han Zuilhof*[,†,§]

[†]Laboratory of Organic Chemistry and [‡]Laboratory of Physical Chemistry and Colloid Science, Wageningen University, Wageningen, The Netherlands

[§]Department of Chemical and Materials Engineering, King Abdulaziz University, Jeddah, Saudi Arabia.

Supporting Information

ABSTRACT: New fluorine-containing terminal alkynes were synthesized and self-assembled onto Si(111) substrates to obtain fluorine-containing organic monolayers. The monolayers were analyzed in detail by ellipsometry, X-ray photoelectron spectroscopy (XPS), Fourier transform infrared reflection absorption spectroscopy (FT-IRRAS), static water contact angle measurements (CA), and atomic force microscopy (AFM). The SAMs exhibit excellent hydrophobicity, with static water contact angles of up to 119° and low critical surface tensions of 5−20 mN/m depending on the number of F atoms per molecule. IRRAS confirmed the formation of highly ordered monolayers, as indicated by the antisymmetric and symmetric stretching vibrations of the CH_2 moieties at 2918−2920 and 2850−2851 cm^{-1}, respectively. Upon increasing the number of fluorine atoms in the alkyne chains from 0 to 17, the adhesion of bare silica probes to the SAMs in air decreases from 11.6 ± 0.20 mJ/m^2 for fluorine-free (F0) alkyne monolayers to as low as 3.2 ± 0.03 mJ/m^2 for a heptadecafluoro-hexadecyne (F17)-based monolayer. Likewise, the friction coefficient decreases from 5.7×10^{-2} to 1.2×10^{-2}. The combination of high ordering, excellent hydrophobicity, low adhesion, and low friction makes these fluoro-hydro alkyne-derived monolayers highly promising candidates for use in high-performance microelectronic devices.

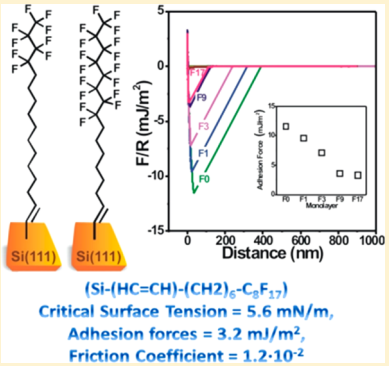

1. INTRODUCTION

Studies on low-adhesion and low-friction surfaces are particularly important for high-performance technological devices. One of the great challenges in many microcomponent devices, such as micro- and nanoelectro-mechanical systems (MEMS and NEMS), is to reduce adhesion to and friction on surfaces as much as possible while keeping the surface highly robust and resistant to wear. The typical dimensions of MEMS and NEMS are a few to several hundreds of micrometers, and they are primarily made from silicon. On these small scales, surface properties such as van der Waals and capillary forces greatly influence the performance of these mechanical systems.[1−3] Without suitable surface modification, Si shows high friction, adhesion, and wear.[4−6] Therefore, several types of thin films have been investigated as coatings for Si with enhanced tribological properties of silicon.[7] In particular, thin organic fluorocarbon−hydrocarbon films have been found to produce low-adhesion and low-friction lubricants.[8−12] In practice, poly(tetrafluoroethylene) (PTFE) is now the primary coating material in many microelectro-mechanical systems.[5] However, these films are not covalently bound to silicon and are therefore prone to wear. Moreover, PTFE films are relatively thick, which may still lead to high adhesion and friction forces when high loads are applied and the films are compressed. Here, we report on ultrathin covalently bound fluoro-hydro alkyne-derived monolayers as high-quality, low-adhesion, and low-friction surface coatings on silicon for use in microcomponent devices.

Densely packed organic monolayers, which are covalently bound via Si−CH═C linkages to crystalline silicon surfaces without an interfacial silicon oxide (SiO_2) layer, are receiving increasing interest[13−15] mainly because of the potential of Si−C bound monolayers for applications in micro- and nanoelectronics as well as in biochemical sensors.[16−22] This field has recently been reviewed.[23] With the advent of nanotechnology, lubricating monolayers are highly desired because they are covalently attached to the substrate and therefore are not easily damaged and even if they break they do not yield particulates that may cause damage. Among the different organic monolayers grafted onto the surface, fluorinated organic thin films have drawn much attention for their outstanding chemical stability, thermal stability, unique wettability, and nonadhesive properties.[24,25] On the nanometer scale, the physical state of thin-film systems may be influenced by a number of forces, including intermolecular interactions between molecules making up the film,[26] surface interactions in adsorbed films, and solvent interactions in detached film systems.[27]

Received: September 28, 2012
Revised: November 27, 2012
Published: December 12, 2012

The formation of a dipole between the last fluorinated carbon ($R-CH_2-CF_2-R^1$) and the first methylene group ($R-CH_2-CF_2-R^1$) in fluorinated organic monolayers causes the electronegative groups to be oriented normal to the surface. This gives rise to an important decrease in adhesion to and friction of the fluorinated monolayers. In addition, fluorination leads to an enhancement of the hydrophobicity and oleophobicity.[28,29] The diverse effects that varying degrees of fluorination cause and the ratio between fluorocarbons and hydrocarbons are under extensive study with the aim of improving the tribological properties and enhancing the hydrophobicity of these monolayers.[30−32]

A range of synthetic methods has been successfully used to prepare covalently bound monolayers on solid surfaces. For silicon, extensive reviews are provided by Gooding et al.[33,34] and Zuilhof et al.[23,35] The formation of a silicon−carbon bond via hydrosilylation is a key step in the coating of a silicon surface with a monolayer because it greatly improves both the packing and stability of SAMs.[34] Grafting of alkynes onto the Si surface can be achieved in various ways.[36−41] The mildest approach already allows for the preparation of high-quality covalently bound organic monolayers at room temperature.[42] As the assembly on the silicon surface progresses, the interchain steric hindrance of CH_2 and CF_2 becomes dominant and prevents the bonding of alkyl chains to every silicon atom of the substrate. Because the resistance toward oxidation depends on the density of monolayer packing,[15] a technique to develop tightly packed monolayers is desired in order to minimize water penetration, oxide formation, and, consequently, the degradation of the silicon substrate.

In this article, we prepare alkyne-based SAMs, which are known to be stable and to form densely packed monolayers.[23,43] By contrast, alkene-based SAMs, in which a $Si-CH_2-CH_2$ single bond allows for a higher degree of free rotation around the chain axis, give rise to a lower packing density. Apart from the enhanced rotation, the saturation of the carbon chain is another important feature: when an alkyne is attached to silicon, an alkene (Si−CH═C linkage) remains, which takes up a smaller volume and thus causes less interchain repulsion than caused by the $Si-CH_2-CH_2$ linkage that is formed upon attaching an alkene to silicon. The enhanced packing density of alkyne-derived monolayers compared to alkene is also due to the smaller tilt angle with respect to the surface normal and the higher ordering of the remaining alkene moieties, facilitated by attractive $\pi-\pi$ interactions.[15] Finally, it is remarked that the packing density increases with longer carbon chains for alkyne-derived monolayers as well as alkene-derived monolayers.[13,44−46]

In studying the characteristics of our S−CH═C linked monolayers together with the requirements for ultralow surface tension and adhesion properties, we expect that partially fluorinated monolayers on a hydrogenated, oxide-free Si (H−Si) surface will combine several of the highly desirable characteristics strived for in this field. This article presents the synthesis of novel fluoro-hydro alkynes with a varying number of fluorine atoms (no. of F atoms = 0−17) at a constant chain length (C_{16}) (Figure 1) and their application to monolayer formation on oxide-free H−Si(111) surfaces. The resulting monolayers are characterized by ellipsometry, X-ray photoelectron spectroscopy (XPS), Fourier transform infrared reflection absorption spectroscopy (FT-IRRAS), advancing and static water contact angle measurements (CA), and critical surface tension measurements. Subsequently, the adhesion and friction of these monolayers were studied as a function of fluorine content by colloidal probe atomic force microscopy (CP-AFM) to reveal unprecedentedly low surface tensions and adhesion properties.

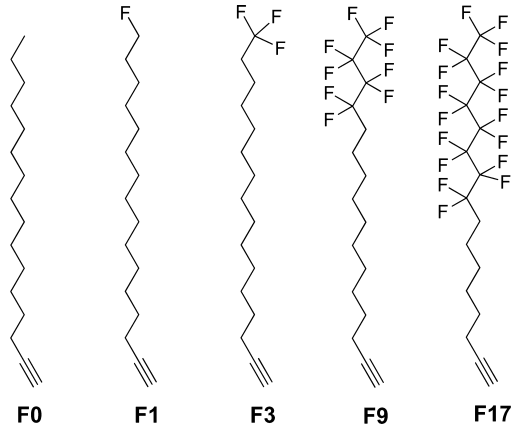

Figure 1. Fluoro-hydro alkynes employed in monolayer formation.

2. EXPERIMENTAL SECTION

2.1. Materials. The synthesis procedures and spectroscopic characterization of hexadec-1-yne (**F0**), 16-fluorohexadec-1-yne (**F1**), 16,16,16-trifluorohexadec-1-yne (**F3**), 13,13,14,14,15,15,16,16,16-nonafluoro-hexadec-1-yne (**F9**), and 9,9,10,10,11,11,12,12,13,13,14,14,-15,15,16,16,16-heptadecafluoro-hexadec-1-yne (**F17**) are described in Supporting Information Schemes S1−S4. For rinsing and contact angle measurements, Milli-Q water (resistivity 18.3 MΩ cm) was used. Hexadecane (C16, 99%), tetradecane (C14, 99%), dodecane (C12, 99%), decane (C10, 99%), heptane (C7, 99%), and hexane (C6, 99%) were used to determine the critical surface tension and were obtained from Aldrich and used as received. Sulfuric acid (Sigma-Aldrich, 95−97%), hydrogen peroxide (Acros Organics, 35%), ammonium fluoride (Riedel-de Haën, 40%, semiconductor grade VLSI Puranal Honeywell 17600), and acetone (Aldrich, semiconductor grade VLSI Puranal Honeywell 17617) were used as received. Silicon wafers were (111)-oriented single-side and doubly polished 500−550 μm thick, phosphorus-doped n-type, and have a resistivity of 2.0−8.0 Ω cm with a 0.2° miscut angle along the ⟨112⟩ plane (Siltronix).

2.2. Hydrogen-Terminated Si(111) Surfaces. Hydrogen-terminated Si(111) surfaces (H−Si) were prepared by chemical etching as previously reported.[45,47] All liquid reagents were continuously purged with a flow of argon. N-type Si(111) was cut into an appropriately sized substrate (10 × 10 mm^2) and subsequently cleaned in a sonication bath with acetone and then with Milli-Q water. The Si wafer was oxidized in freshly prepared piranha solution (H_2SO_4/H_2O_2 3:1) for at least 20 min. After piranha treatment, the substrates were immersed immediately in water and rinsed thoroughly, followed by drying with a stream of argon. Subsequently, the substrates were etched in an argon-saturated 40% aqueous NH_4F solution for 15 min, rinsed with Milli-Q water, and finally dried with a stream of argon.

2.3. Preparation of Fluoro-Hydro Alkyne-Derived Monolayers on Si(111). A three-necked flat-bottomed flask connected to a thin capillary as the argon inlet and to a reflux condenser connected to a vacuum pump was charged with individual neat fluoro-hydro alkyne (Scheme 1), flushed with argon, and heated to 80 °C in order to remove traces of oxygen and moisture. The freshly etched Si(111) substrate was placed in fluoro-hydro alkyne. The reaction was carried out at 80 °C under an argon atmosphere at an argon pressure of 2−5 mbar for 16 h. After the reaction had been stopped, the modified surfaces were rinsed and sonicated with CH_2Cl_2 for 5 min to remove any physisorbed fluoro-hydro alkynes.

2.4. Monolayer Characterization. *2.4.1. Contact Angle Measurements.* Contact angle measurements were performed on a Krüss DSA 100 contact angle goniometer with an automated drop

dx.doi.org/10.1021/la303893u | *Langmuir* 2012, 28, 17690−17700

Scheme 1. Synthesis Procedure Used to Create Fluoro-Hydro Alkynes, with F3 Given as an Example

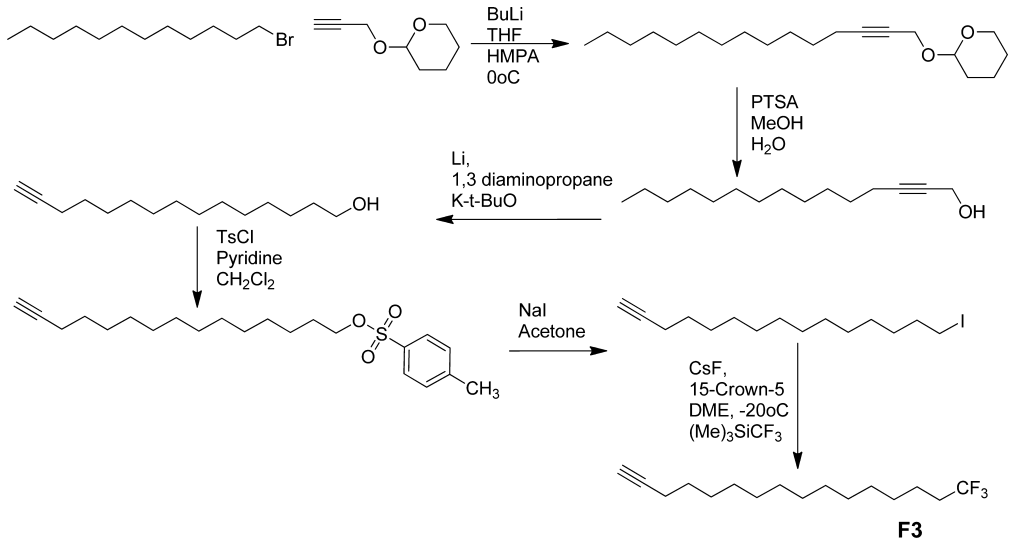

dispenser and image video capture system. The static contact angles of six small droplets (3.0 μL volume of liquid) dispensed on modified silicon surfaces with a microliter syringe with a stainless steel needle (diameter = 0.51 mm) were determined using a Tangent 2 fitting model. The digital drop images were processed by the image analysis system, which calculated both the left and right contact angles from the drop shape with an accuracy of ±1.0°. For advancing contact angle determinations on the same polymer samples, droplets of 1 μL total volume were applied at 10 μL/min and monitored by video recording. Reported angles are averaged over at least five droplets

2.4.2. Ellipsometry. The thickness of the modified silicon surfaces (in the dry state) was measured using a rotating analyzer ellipsometer (Sentech Instruments type SE-400) operating at 632.8 nm (He−Ne laser) with an angle of incidence of 70°. The optical constants of the substrate were determined with a piece of freshly etched H−Si(111) (n = 3.819 and k = 0.057). The thicknesses of the monolayers were determined with a planar three-layer (ambient, monolayer, and substrate) isotropic model with a refractive index for the organic monolayers of 1.46 (**F0**), 1.44 (**F1**), 1.40 (**F3**), 1.38 (**F9**), and 1.35 (**F17**).[48] Each reported value of the layer thickness is the average of eight measurements taken at different locations on the substrate with an error of <1 Å.

2.4.3. Atomic Force Microscopy. Force measurements are performed on a Nanoscope IIIA AFM (Digital Instruments) equipped with a PicoForce scanner. Spherical silica particles (R = 3.0 μm, rms roughness value of 6.83 ± 2.06 nm)[49] were attached to triangular standard silicon nitride cantilevers (Bruker probes, NP-B, spring constant between 0.10 and 0.16 N/m) using Norland optical adhesive 61 and cured with UV light (365 nm). Before use, the colloidal probes were cleaned with excess ethanol followed by 5 min of air plasma cleaning. Both adhesion and friction measurements were carried out in air at a relative humidity of 44 ± 2%.

Adhesion forces were measured using a scan range of 1.0 μm for modified surfaces and 10 μm for oxide surfaces at a scan rate of 0.5 Hz. At least 200 separate force curves were recorded for every surface. For each cantilever, the normal spring constant was determined using the thermal tuning method introduced by Hutter and Bechhoefer,[50] correcting for the nonideality of the spring and the fact that the deflection sensitivity was measured for a supported cantilever.[51] The overall error in the measured adhesion forces is the sum of uncertainties in the voltage measurement, deflection sensitivity, and spring constant and was estimated to be ±10%.[32,52]

Friction forces were obtained from the trace and retrace of 5 × 5 μm^2 lateral force images under varying normal loads (F_N = 0−80 nN). The lateral force images are measured at a constant speed of 5 μm/s under a 90° angle with respect to the cantilever's long axis. The average lateral force difference signal ($[\mu_{trace} - \mu_{retrace}]/2$, in V) was converted directly into friction force, following the method of Liu et al.[53] Cantilevers were calibrated using the reversible bending of an 8.9 -μm-thick glass fiber, leading to a lateral conversion factor of approximately 17.7 nN/V. The overall error in the conversion factor determined in this way was estimated to be 15%.[53]

2.4.4. X-ray Photoelectron Spectroscopy (XPS). XPS measurements were performed using a JPS-9200 photoelectron spectrometer (JEOL, Japan). A monochromatic Al Kα X-ray source ($h\nu$ = 1486.7 eV, 12 kV, 20 mA) using an analyzer pass energy of 10 eV was used. The base pressure in the chamber during measurements was 3 × 10^{-7} Torr, and spectra were collected at room temperature. The intensity of the XPS core-level electron was measured as the peak area after standard background subtraction according to the linear procedure. The takeoff angle φ (angle between sample and detector) of 80° is defined to a precision of 1°. The typical sample size was 1 × 1 cm^2. All XPS spectra were evaluated using the Casa XPS software (version 2.3.15). The symmetrical GL(30) line shape was employed, which consists of a Gaussian (70%) and a Lorentzian (30%) component. The fwhm of each component was constrained to ∼1.0 eV. The relative areas of each component peak were fixed by the stoichiometry of the main hydrocarbon (CH_2), which was assigned as aliphatic carbon with a binding energy of 285.00 eV.

2.4.5. Fourier Transform Infrared Reflection Absorption Spectroscopy (IRRAS). IRRA spectra were recorded on a Bruker Tensor 27 FT-IR spectrometer using a variable-angle reflection unit (Auto Seagull, Harrick Scientific). A Harrick grid polarizer was installed in front of the detector and was used to record spectra with p-polarized (parallel) radiation with respect to the plane of incidence at the sample surface. All spectra were obtained at an incident angle of 68° (2048 scans). The resolution was set at 2 cm^{-1} per modulation center. The final spectra were obtained using a piranha-oxidized reference surface as the background. Data were collected as differential reflectance versus wavenumber. All spectra were recorded at room temperature under a dry atmosphere.

2.4.6. Molecular Modeling. For the molecular modeling study, the same method is followed as reported by Scheres et al.[43,54] In short, Materials Studio software (version 5.0) was used to construct and optimize the monolayers. All monolayers were formed from five standard cells containing a decenyl chain (representing one of the alkynes) attached in an all-trans conformation to four Si atoms. The Si atoms represent the first four layers of the Si substrate obtained by cleaving a Si crystal along the (111) plane. The structures were placed in a box to obtain the standard cells. The standard cells were copied in the directions of the Si substrate to form larger unit cells. By replacing some of the attached chains with hydrogen atoms, different substitution patterns and substitution percentages were obtained. All unit cells were finally copied to form the final large simulation cells

dx.doi.org/10.1021/la303893u | *Langmuir* 2012, 28, 17690−17700

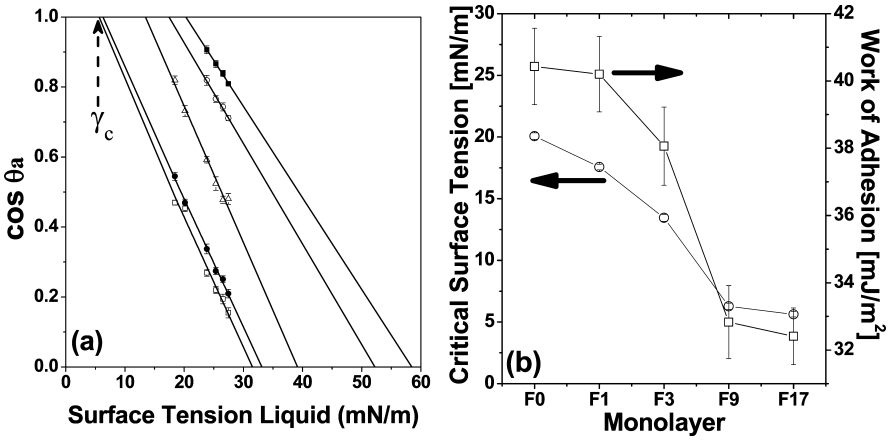

Figure 2. (a) Zisman plot showing the linear regression of cos θ vs different *n*-alkanes (from C6 to C16) on **F17** (□), **F9** (●), **F3** (△), **F1** (○), and **F0** (■) monolayers on H-terminated Si(111). The line coefficient $r^2 = 0.98 \pm 0.01$ indicates a high degree of confidence. (b) Critical surface tension (○) and work of adhesion (■) on SAMs derived from the hexadecyne series as a function of the total number of fluorine atoms per chain. Critical surface tensions (γ_c) are obtained from extrapolation to cos θ = 1 at 24 ± 2 °C.

representing the whole modified Si surface. The unit cells and the large simulation cells were optimized using a polymer consistent force field (PCFF) with the Smart Minimizer routine and high-convergence criteria. Periodic boundary conditions were applied.

3. RESULTS AND DISCUSSION

3.1. Synthesis of Fluoro-Hydro Alkynes. The synthesized fluoro-hydro alkynes are depicted in Figure 1. Fluorine-free 1-hexadecyne (**F0**) was obtained by the tosylation of 1-tetradecanol, followed by nucleophilic substitution with lithium acetylide. **F3** was synthesized in six steps (Scheme 1; full experimental details in Supporting Information), consisting of the coupling of THP-protected propargyl alcohol to 1-bromododecane, followed by deprotection of the THP-group affording pentadec-2-yn-1-ol. The isomerization of pentadec-2-yn-1-ol afforded the terminal alkyne, which was again tosylated and subsequently converted to the corresponding iodide to increase the reactivity for the final reaction with Me_3SiCF_3 to yield **F3**. A similar procedure was followed in preparing **F1** from commercially available hexadec-7-yn-1-ol. After isomerization and tosylation, treatment with KF afforded **F1**. Heptadecafluoro alkyne **F9** was obtained via a four-step reaction (Supporting Information Scheme S1). The radical chain addition of 1,1,1,2,2,3,3,4,4-nonafluoro-4-iodobutane to 9-decene-1-ol afforded 11,11,12,12,13,13,14,14,14-nonafluoro-9-iodotetradecan-1-ol, and was followed by the reduction of the iodide to give reduced 11,11,12,12,13,13,14,14,14-nonafluorotetradecan-1-ol. The tosylation of 11,11,12,12,13,13,14,14,14-nonafluorotetradecan-1-ol was followed by nucleophilic substitution with lithium acetylide to obtain fluoro-hydro alkyne **F9**. **F17** was synthesized following the same procedure but starting with 1,1,1,2,2,3,3,4,4,5,5,6,6,7,7,8,8-heptadecafluoro-8-iodooctane and 5-hexen-1-ol.

3.2. Monolayer Formation. In our search for a mild and generally applicable method for grafting the newly synthesized fluoro-hydro-containing alkynes onto Si substrates, we investigated different reaction times and temperatures (data not shown). Typically, the Si substrate was immersed in neat alkyne under oxygen-free and water-free conditions. Although high-quality monolayers were formed on Si(111) with **F0** even at room temperature under ambient light,[42] the modification with fluorinated alkynes was not completed under these conditions and physisorption dominated on the basis of weak van der Waals interaction or hydrogen bonding in C−F···H−C.[55] Hence, the grafting of the fluorinated alkynes required reaction conditions of at least 80 °C for 16 h.

Advancing and static water contact angle measurements were determined for all monolayers (Supporting Information Table S1). The hexadecyne (**F0**)-based monolayer displayed a static water contact angle of 110°, in agreement with earlier observed values.[42] The hydrophobicity of the SAMs based on **F1**−**F17** are typical of the presence of fluorinated moieties.[28] The water contact angle increases with the increasing number of fluorines in the monolayer (static water contact angle up to 119° for **F17**) and compares favorably with that of PTFE (115°). For **F9** and **F17**, higher contact angles were observed because of the weak dipole−dipole interaction between the CF_3 terminus and water molecules. In comparison, a PTFE surface displays a lower static water contact angle because the CF_2 groups are less capable of reducing the surface energy than CF_3 groups.[56] The lower polarizability of fluorine compared to that of hydrogen leads to very weak van der Waals interactions among the CF_3 terminus and polar water molecules.[57] There have been a number of studies on the influence of terminal groups.[58,59] Colorado et al. obtained for the Au···S−$(CH_2)_{15-x}(CF_2)_xCF_3$ series of monolayers a smaller contact angle (108°) for x = 0 (comparable to that for our **F3** monolayer, θ = 113°).[28] This smaller contact angle is likely due to a more horizontal organization of the CH_2−CF_3 terminus, thus exposing the CH_2 moiety. In our case, the monolayer is likely more organized, presenting only the CF_3 group head up, yielding a higher hydrophobicity.

From the advancing water contact angle, the apparent work of adhesion can be calculated. Figure 2 shows how the work of adhesion decreases with an increasing number of fluorine atoms. The strongest decrease occurs between **F3** and **F9**, as discussed above. Between **F9** and **F17**, little change is observed.

A similar trend is found in the critical surface tension of the monolayers. Critical surface tensions are obtained from Zisman plots of static contact angles of a series of linear alkanes on the monolayers. A Zisman plot can be used to investigate the surface energy of a low-energy solid surface.[60] When the surface energy of the solid is comparable to that of the liquid, a transition from partial to complete wetting is observed. Surfaces with very low surface energies are difficult to wet and may never achieve complete wetting.

dx.doi.org/10.1021/la303893u | *Langmuir* 2012, 28, 17690−17700

Table 1. XPS Data Atomic C/Si Ratio and XPS and Ellipsometry Thickness

monolayer	C/Si	C/F ratio theory	C/F ratio exp	XPS thickness (nm)	ellipsometry thickness (nm)	refractive index
F0	40.9/59.1			2.07	2.09	1.46
F1	38.7/61.3	16.0	15.0	2.01	2.02	1.44
F3	38.4/61.6	5.3	5.2	1.91	1.95	1.40
F9	37.2/62.8	1.8	1.9	1.84	1.91	1.39
F17	37.8/62.2	0.9	1.0	1.89	1.93	1.35

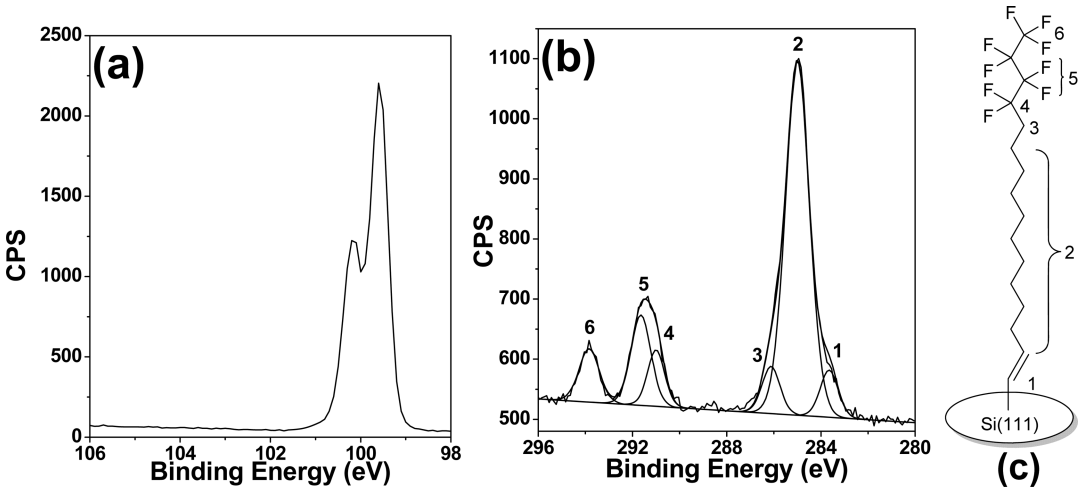

Figure 3. High-resolution XPS data of an **F9**-based monolayer on an oxide-free H−Si(111) surface. (a) Si 2p and (b) C 1s. (c) Schematic representation of the **F9** monolayer on Si(111).

In that case, measuring the wetting contact angle (θ) for different values of the liquid surface tension (γ_L) and extrapolating to cos θ = 1 (i.e., complete wetting) will yield a critical surface tension (γ_c) that is a measure for the solid surface energy and an essential parameter in many practical applications.[61] In general, the critical surface tension and the details of the extrapolation depend on the molecular characteristics of the liquid.[61] However, in a homologous series of simple molecular liquids such as *n*-alkanes, the van der Waals forces dominate the liquid surface energy, and Zisman found that cos θ depends linearly on γ_L.[60] Using this approach, Zisman determined critical surface tensions for a variety of solids with a low-energy surface. The lowest critical surface tension found was 6 mN/m for condensed monolayers of perfluorolauric acid on platinum, whereas Teflon has a critical surface tension of 18.5 mN/m.

The monolayers in this study stand out by displaying extraordinarily low surface tensions. Figure 2a shows Zisman plots for fluoro-hydro alkyne-derived monolayers **F0**−**F17** using a homologous series of *n*-alkanes. In all cases, a linear relationship is found between cos θ and γ_L, in agreement with the original findings of Zisman.[60] The corresponding critical surface tensions are shown in Figure 2b. Surfaces with a low critical surface tension are expected to suffer least from adhesion to the surface, which is desirable in many microelectronic devices. First, the critical surface tension for **F0** is found to be 20.1 mN/m, which is lower than characteristic values reported for CH_3 termination in the literature (22−24 mN/m),[62] revealing the high organization of the monolayer. Increasing the number of F atoms in the monolayer further decreases the critical surface tension to 5.6 ± 0.21 mN/m for **F17**, which is, as far as we know, currently the lowest for any solid surface. Consequently, only condensed inert gases would show complete wetting on this surface.[60,63]

Table 1 summarizes monolayer thicknesses measured by ellipsometry as well as XPS.[13] The observed refractive index (RI) of the **F17** monolayer on Si(111) is close to that of the analogous F_{17} silane reported by Geer et al.[48] Monolayers prepared from compounds **F9** and **F17** display slightly lower thicknesses than those obtained from **F0**, **F1**, and **F3.** The relaxed fluoro-hydro alkyne molecules in the SAMs are most likely not straight but helical and bent, similar to fluorinated alkyl thiols on Au. Such monolayers were reported to display tilt angles of 30−35° with respect to the surface normal.[31,64,65] The lower thicknesses may also relate to differences in the effective cross-sectional area of the $-CF_2-CF_3$ and $-CH_2-CH_3$ moieties (28 and 18 Å^2, respectively) and fit it less optimally with the intersite distances on the Si(111) surface.[66]

The fluoro-hydro alkyne-derived monolayers were also analyzed by XPS, and the resulting C 1s and Si 2p high-resolution spectra of an **F9**-based monolayer are depicted in Figure 3. The peak labels in the spectra correspond to the carbon atoms having different environments in the modified monolayer, which was deconvoluted into six distinct components. Hydrocarbon CH_2 C 1s (signal 2) calibrated at a binding energy of 285.0 eV corresponds to carbon atoms involved in CH_2 moieties of **F9**, whereas signal 1 at 283.6 eV is assigned to the carbon bound to the less electronegative Si.[42] The relative intensity of this Si−C signal is $\sim^1/_{16}$ of the total C signal, in line with expectations. The C 1s signal (3) at 286.1 eV corresponds to the methylene carbon atom involved in the $-CF_2-CH_2-$ group. The shoulder peak observed at 290.9 eV corresponds to the $-CF_2-CH_2-$ group (4). The C 1s signal (5) at 291.6 eV corresponds to the other CF_2 groups, whereas the highest binding energy (293.8 eV) is observed for the terminal CF_3 group (Figure 3b).[63] This assignment is in excellent agreement with computational C 1s and F 1s XPS

dx.doi.org/10.1021/la303893u | *Langmuir* 2012, 28, 17690−17700

data obtained from B3LYP/6-311G(d,p) calculations (Supporting Information Figure S1).[67]

The Si 2p high-resolution spectrum (Figure 3a) shows binding energies of the Si $2p_{1/2}$ and Si $2p_{3/2}$ doublet at 100.1 and 99.5 eV, respectively. Importantly, no contribution related to oxide or suboxide species in the energy range of 101−104 eV was observed, indicating the oxide-free nature of the silicon substrate underneath this partially fluorinated monolayer. Whereas excellent surface passivation has been shown before for alkyne-derived **F0** monolayers,[13] apparently fluorination does not hamper the formation of a fully surface-covering monolayer.

3.3. Infrared Reflection−Absorption Spectroscopy. Qualitative differences in the conformational order of the alkyl chains in the monolayers were evaluated using infrared reflection−adsorption spectroscopy (IRRAS) by monitoring the antisymmetric and symmetric CH_2 stretching vibrations (Figure 4A).[13,68,69] For increases in fluorine content from **F0** to **F17**, the SAMs exhibited slightly increasing values for the antisymmetric CH_2 stretching vibrations from 2918 to 2920 cm^{-1} as well as symmetric stretching vibrations ranging from 2850 to 2851 cm^{-1}. The low values observed for **F0** are, as reported before,[13] attributed to the high degree of short-range ordering in these monolayers. Because higher values of these peak frequencies are typically correlated with diminished ordering, it may be thought that the higher values observed for **F17** display a reduced ordering. However, another electronic factor comes into play here. The increased electronegativity of the chain yields an upward shift of the CH_2 stretching vibrations, as exemplified by B3LYP/6-311G-(d,p) data obtained for frequencies of the C−H stretching vibrations of model compounds $CH_3-(CH_2)_7-(CH_2)_7CH_3$ (i.e., *n*-hexadecane) and $CH_3-(CH_2)_7-(CF_2)_7CF_3$ using scaled (0.9679)[70] optimized B3LYP/6-311G(d,p) data. As can be seen (Figure 4B), fluorination by itself decreases the C−H stretching vibrational frequencies by approximately 3 cm^{-1}. If one thus compensates for this electronic effect on the CH_2 stretching vibrations, the degree of ordering in our fluorinated monolayers seems to equal that observed for **F0**, pointing to highly ordered monolayers throughout the entire fluoro-hydro alkyne series. This high ordering, of course, does not imply identical conformations because the **F9** and **F17** chains may well display helical conformations.[71]

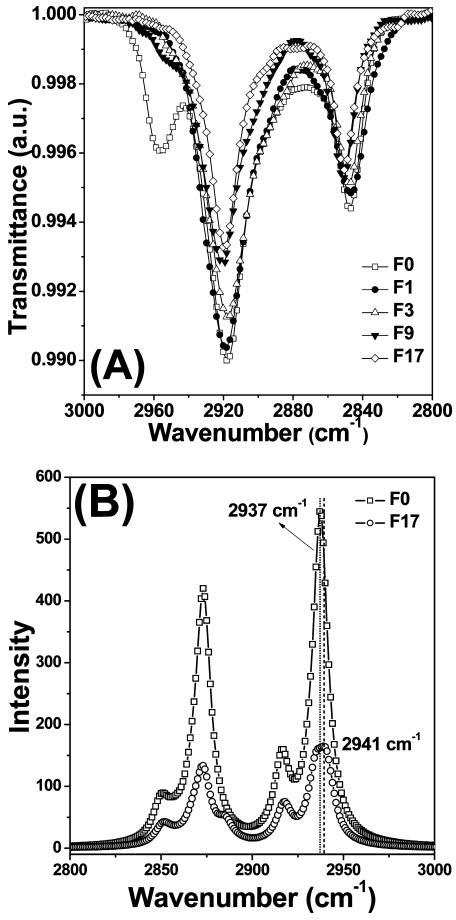

Figure 4. (A) IRRAS spectra (between 2800 and 3000 cm^{-1}) for fluorinated monolayers on H−Si(111). (B) DFT calculations of relevant vibrational frequencies of $CH_3-(CH_2)_7-(CX_2)_7CX_3$ (X = H and F) optimized by B3LYP/6-311G(d,p) using a scaling factor of 0.9679.

3.4. Adhesion and Friction. To assess the adhesion and friction characteristics of the modified Si(111) surfaces, atomic force microscopy was used. Both adhesion to and friction on surfaces greatly influence the performance of microelectronic devices. Colloidal probe AFM allows us to measure both properties with high accuracy. The colloidal probe acts as a model solid object that can interact with the modified surfaces. Previously, covalently bound alkene SAMs and adsorbed fluorine-containing surface coatings have been shown to reduce adhesion and increase lubrication significantly in solution.[52,72] However, most devices operate in air or vacuum, where adhesion is expected to be much larger. Moreover, capillary condensation may occur between surfaces that are hydrophilic enough, leading to even stronger adhesive interactions. Under these conditions, a candidate surface coating should still effectively reduce adhesion and provide sufficient lubrication. Therefore, fluoro-hydro alkyne-derived monolayers were subjected to the most stringent adhesion and friction test by carrying out the AFM measurements in air with a smooth silica probe as a hydrophilic solid particle.

The fluorinated monolayers in this study display very low adhesion forces. Figure 5 shows the adhesion of a silica probe particle to the monolayers when the surfaces are compressed at a load of 10 nN. Adhesion forces decrease with increasing fluorine content in the monolayers from 35 nN (11.6 ± 0.20 mJ/m^2) for the **F0**-based monolayer to as low as 9.8 nN (3.2 ± 0.03 mJ/m^2) for the **F17**-based monolayer. As far as we know, this is the lowest adhesion force observed for any flat surface. This low adhesion is attributed to the high degree of ordering in the monolayer, which allows little reorganization within the monolayer to increase attractive interactions between the monolayer and the probe. Only in the case of **F0** monolayers was a small nonzero attraction measured upon approaching the surfaces.

The measured adhesion originates from van der Waals interactions between the probe particle and the fluoro-hydro alkyne-coated Si(111) surface. Stable water capillary bridges cannot be formed because of the high water contact angle of the SAMs and the low relative humidity.[73] The low adhesion forces and thus low surface energies of the **F9**- and **F17**-based monolayers confirm the low polarizability of the terminal CF_2-CF_3 groups. The **F9**- and **F17**-based monolayers show lower adhesion than do $-(CH_2)_n-CF_2-CF_3$ SAMs on silica surfaces and are even comparable to rough surfaces of PEG-grafted and

dx.doi.org/10.1021/la303893u | *Langmuir* 2012, 28, 17690−17700

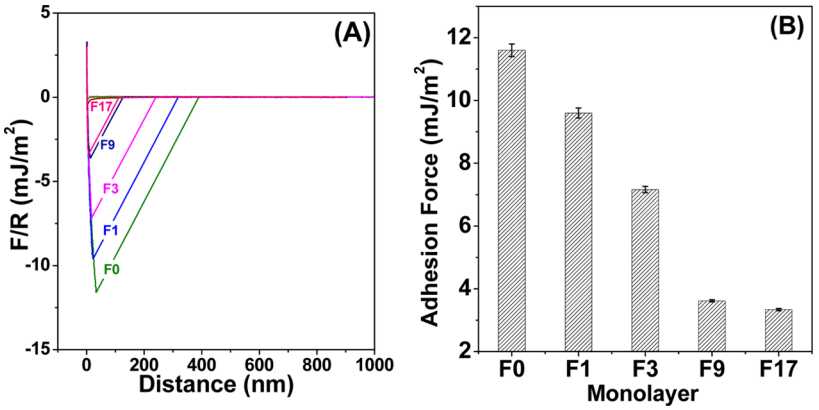

Figure 5. (A) Representative force−distance curves for SAMs with different fluorinated monolayers. In all cases, a load of 10 nN is applied. (B) The adhesion force, defined as the minimum in the force−distance plot, for different monolayers.

fluorinated nanoparticles in air.[72] Clearly, the high quality of these monolayers further reduces the surface energy and leads to minimal adhesion. Combining these monolayers with structured surfaces would thus be very interesting for the construction of robust superhydrophobic surfaces.

The low thickness of the monolayers compared to that of other PTFE coatings[74] leads to limited compressibility, and this suggests that the adhesion will not increase significantly when the applied load is increased. Figure 6 shows the increase in adhesion with increasing load for all monolayers in air. Indeed, adhesion increases only slightly (30%), with the increase being largest for the **F0**-based monolayer. The increasing adhesion originates from the elastic compression of the surfaces, which yields a larger contact area between the solid probe and the monolayers. The JKR model can be used to predict the load deformation of compressed surfaces when their interaction is governed by short-range adhesion only.[75] In this case, the total compression is determined by three materials with very different elastic moduli: the silica probe, the Si(111) substrate, and the fluoro-hydro alkyne-derived monolayer. Therefore, a two-layer substrate JKR model was used in which a transition function describes the change in the elastic modulus of the substrate from the top of the SAM (150−300 MPa) to deep inside the Si(111) (160 GPa).[76] The solid lines in Figure 6 represent fits of the data to this modified JKR model with a fixed layer thickness of 2.0 nm in all cases. The elastic modulus of the monolayer decreases with increasing fluorine content by a total factor of 2 (from **F0** to **F17**). This decrease may be explained by the higher order and crystallinity of **F0**-, **F1**-, and **F3**-based monolayers compared to those of **F9**- and **F17**-based monolayers. In addition, the model gives a prediction for the compression of the SAM and the area of contact between the silica probe and the SAM as a function of the normal load. Using these values, we can calculate the work of adhesion between the silica probe and the fluoro-hydro alkyne-coated Si(111) and an effective Hamaker constant using the Derjaguin approximation. A typical indentation of the SAM at a normal load of 10 nN is 1.3 nm, leading to a contact area of 0.030 μm^2. Combined with the adhesion forces in Figure 5, the effective Hamaker constant is found to decrease from $15.4k_BT$ for the **F0**-derived monolayer to $5.1k_BT$ for the monolayer obtained from **F17**. There is good agreement between the Hamaker constant for the **F0** monolayer with the theoretical prediction for the interaction between a silica probe and Si(111) covered with a crystalline hydrocarbon layer.[77]

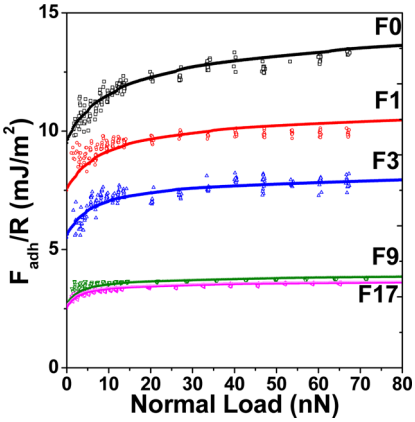

Figure 6. Adhesion forces of a colloidal silica probe as a function of the normal load for different monolayers. Solid lines are fits of the data with a JKR model of a soft layer with 1.8 nm thickness on top of H−Si(111).

Besides adhesion, the friction of laterally moving or rolling objects on the surfaces of microelectronic devices is an important aspect that governs their performance. Minimal friction coefficients or high lubrication are desirable. The lateral friction force on the fluorinated monolayers was measured using the same colloidal probe setup as for the adhesion measurements. The load was varied from 0 to 75 nN, and the lateral friction was recorded on several 5 × 5 μm^2 areas (Supporting Information Figure S2). The mean friction forces are depicted in Figure 7. The friction forces follow an apparent Gaussian distribution around the mean values, and the typical relative standard deviation is shown in Figure 7A. Variations between the mean friction forces on three independently modified surfaces were found to be smaller than the variations in the friction force on one surface. The friction coefficients are calculated from the slopes of the data in Figure 7B. At zero load, a small but nonzero friction value results from the adhesion between the probe and monolayer. The magnitude of this apparent adhesion, obtained by extrapolating to zero friction force, is lower than the adhesion found in normal force measurements (Figure 6). This is probably due to the weak stick−slip nature of the frictional motion, for which the mean frictional force can be lower than for smooth sliding.[78,79]

This friction at zero load decreases with increasing fluorine content, in agreement with the adhesion measurements. For

dx.doi.org/10.1021/la303893u | *Langmuir* 2012, 28, 17690−17700

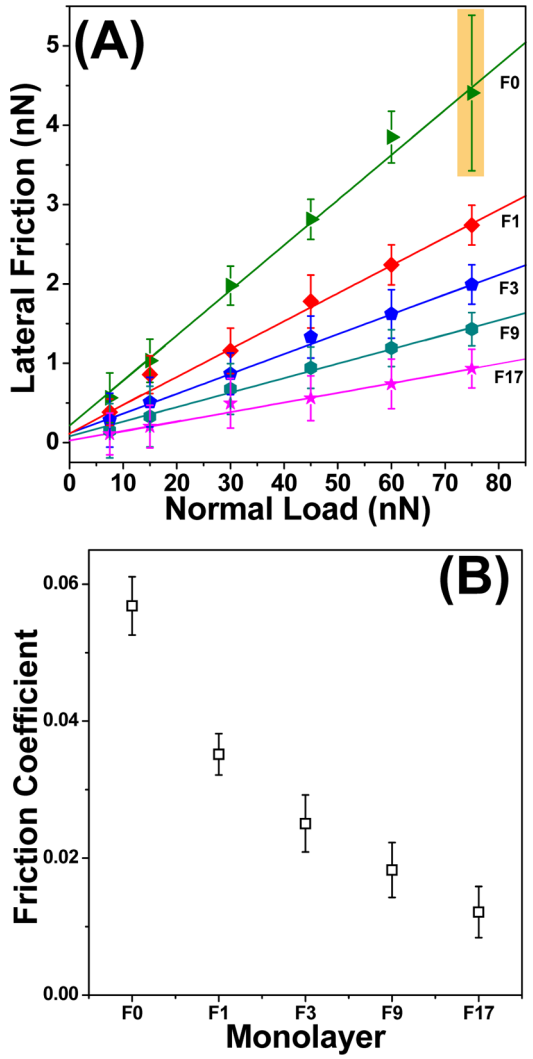

Figure 7. (A) Lateral friction force of fluorinated SAMs on Si(111) as a function of the applied normal load. The error bars represent the standard deviation in mean friction force between three independently modified surfaces. The highlighted error bar at a normal load of 75 nN shows the relative variation in the friction force on a single surface (Supporting Information Figure S2). (B) The friction coefficients, obtained from the slope of the friction force versus normal load, for different monolayers.

F0-based monolayers, a friction coefficient of 5.7×10^{-2} is found, in good agreement with the results for SAMs on gold.[52] With increasing fluorine content in the monolayers, the friction coefficient decreases to the rather low value of 1.2×10^{-2} for **F17**-based monolayers. These values are comparable to the data reported for $C_{16}H_{33}$ thiol monolayers on Au (3.0×10^{-3}) and $C_{16}H_{33}$ alcohol monolayers on Si (1.3×10^{-2}).[80] Interestingly, for SAMs on Au the friction coefficient increases with an increase in fluorination[81] or shows no change,[52] in marked contrast to our data. Kim et al. have summarized the factors that can influence friction: (i) chemical structure and binding of an organic molecule to a substrate, (ii) packing density and monolayer order, (iii) gauche conformation and or surface coverage, (iv) mechanical properties such as elastic constant and rigidity of the monolayer, (v) terminal polar or nonpolar functional groups, and (vi) surface dipole orientations.[66,82] In this case, the fluorine-rich monolayers (especially **F9** and **F17**) are expected to have a lower polarizability on their surface as a result of the dipole orientation of the last fluorinated carbon and the first methylene group ($R-CH_2-CF_2-R^1$), are densely packed, and display a high short-range organization, leading to an overall low friction coefficient.

3.5. Molecular Modeling. To substantiate the optimum substitution percentages of the fluoro-hydro alkyne-derived monolayers on H–Si(111) and to investigate the structural differences between different fluorinated monolayers, models of the monolayers were studied by molecular mechanics (Supporting Information Figure S3 and S4). Packing energies of SAMs on H–Si(111) for different surface coverages are depicted in Figure 8. The average packing energy per chain was

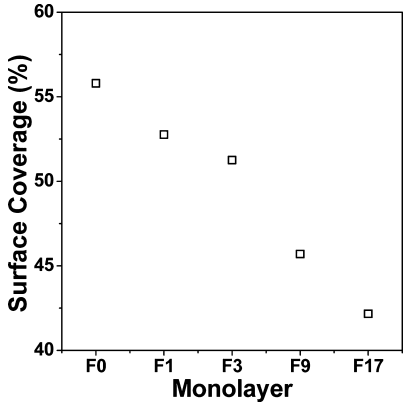

Figure 8. Surface coverage for fluoro-hydro alkyne-derived monolayers **F0**–**F17** on H–Si(111).

then calculated according to the literature,[43,54] and the optimal surface coverage was obtained after fitting to a parabolic function. The optimum surface coverage decreases from 56% for **F0** to 42% for **F17** because of the larger cross section of the CF_2/CF_3 moieties. These values are confirmed by the experimentally determined monolayer thicknesses (displayed in Table 1), with a clear trend in the direction of greater surface coverage for **F0** as compared to that for **F17**.

4. CONCLUSIONS

Partially fluorinated Si–CH=C bound monolayers on oxide-free Si(111) surfaces display an extremely low surface tension and adhesion. Such self-assembled organic monolayers are uniform, densely packed, and characterized by a high degree of short-range ordering. This set of properties yields a highly uniform upward presentation of CF_3 moieties, yielding a low interaction with the outside world as evidenced by a critical surface tension of 5.6 ± 0.21 mN/m, an adhesion force of 3.2 ± 0.03 mJ/m^2, and a friction coefficient of 1.2×10^{-2} for the **F17** monolayer ($Si-(HC=CH)-(CH_2)_6-C_8F_{17}$). Each of these values is either the lowest currently measured for any flat surface or close to it. The present study suggests that fluoro-hydro alkyne-derived monolayers on silicon surfaces significantly expand the scope of strong covalently bound nanometer monolayers and display significant potential in MEMS/NEMS applications.

■ ASSOCIATED CONTENT

Supporting Information

Synthesis and characterization of fluorinated alkynes, contact angle, molecular modeling, DFT calculations of the chemical shifts in XPS of the carbon atoms, full citation for Gaussian 09,

dx.doi.org/10.1021/la303893u | *Langmuir* 2012, 28, 17690–17700

and AFM friction image. This material is available free of charge via the Internet at http://pubs.acs.org

AUTHOR INFORMATION

Corresponding Author

*Phone: +31-317-482361. E-mail: han.zuilhof@wur.nl.

Notes

The authors declare no competing financial interest.

ACKNOWLEDGMENTS

We thank Dr. Mabel Caipa Campos, Radostina Manova, and Dr. Luc Scheres for discussions and help with the surface modifications. Dr. Marcel Giesbers, Barend van Lagen, Frank Claassen, and Elbert van der Klift are acknowledged for instrumental assistance. This project was partially funded by the Marie Curie European Union FP7 project "Surface Physics for Advanced Materials" research program and by ASML, The Netherlands.

REFERENCES

(1) Butt, H.-J.; Kappl, M. *Surface and Interfacial Forces*; Wiley-VCH: Weinheim, Germany, 2010.

(2) Israelachvili, J. N. *Intermolecular and Surface Forces*, 3rd ed.; Academic Press: Burliington, MA, 2011; pp 253−289.

(3) Kristiansen, K.; Zeng, H.; Wang, P.; Israelachvili, J. N. Microtribology of Aqueous Carbon Nanotube Dispersions. *Adv. Funct. Mater.* **2011**, *21*, 4555−4564.

(4) Ren, S. L.; Yang, S. R.; Wang, J. Q.; Liu, W. M.; Zhao, Y. P. Preparation and Tribological Studies of Stearic Acid Self-assembled Monolayers on Polymer-Coated Silicon Surface. *Chem. Mater.* **2004**, *16*, 428−434.

(5) Palacio, M.; Bhushan, B. Ultrathin Wear-Resistant Ionic Liquid Films for Novel MEMS/NEMS Applications. *Adv. Mater.* **2008**, *20*, 1194−1198.

(6) Prioli, R.; Jacobsohn, L. G.; da Costa, M.; Freire, F. L. Nanotribological Properties of Amorphous Carbon-Fluorine Films. *Tribol. Lett.* **2003**, *15*, 177−180.

(7) Tsukruk, V. V. Molecular Lubricants and Glues for Micro- and Nanodevices. *Adv. Mater.* **2001**, *13*, 95−108.

(8) Bhushan, B.; Israelachvili, J. N.; Landman, U. Nanotribology: Friction, Wear and Lubrication at the Atomic Scale. *Nature* **1995**, *374*, 607−616.

(9) McGuiggan, P. M. Friction and Adhesion Measurements Between a Fluorocarbon Surface and a Hydrocarbon Surface in Air. *J. Adhes.* **2004**, *80*, 395−408.

(10) Socoliuc, A.; Gnecco, E.; Maier, S.; Pfeiffer, O.; Baratoff, A.; Bennewitz, R.; Meyer, E. Atomic-Scale Control of Friction by Actuation of Nanometer-Sized Contacts. *Science* **2006**, *313*, 207−210.

(11) Carpick, R. W.; Salmeron, M. Scratching the Surface: Fundamental Investigations of Tribology with Atomic Force Microscopy. *Chem. Rev.* **1997**, *97*, 1163−1194.

(12) Mo, Y. F.; Turner, K. T.; Szlufarska, I. Friction Laws at the Nanoscale. *Nature* **2009**, *457*, 1116−1119.

(13) Scheres, L.; Giesbers, M.; Zuilhof, H. Organic Monolayers onto Oxide-Free Silicon with Improved Surface Coverage: Alkynes versus Alkenes. *Langmuir* **2010**, *26*, 4790−4795.

(14) Ng, A.; Ciampi, S.; James, M.; Harper, J. B.; Gooding, J. J. Comparing the Reactivity of Alkynes and Alkenes on Silicon (100) Surfaces. *Langmuir* **2009**, *25*, 13934−13941.

(15) Puniredd, S. R.; Assad, O.; Haick, H. Highly Stable Organic Monolayers for Reacting Silicon with Further Functionalities: The Effect of the C-C Bond Nearest the Silicon Surface. *J. Am. Chem. Soc.* **2008**, *130*, 13727−13734.

(16) Halik, M.; Klauk, H.; Zschieschang, U.; Schmid, G.; Dehm, C.; Schutz, M.; Maisch, S.; Effenberger, F.; Brunnbauer, M.; Stellacci, F. Low-Voltage Organic Transistors with an Amorphous Molecular Gate Dielectric. *Nature* **2004**, *431*, 963−966.

(17) Zigah, D.; Herrier, C.; Scheres, L.; Giesbers, M.; Fabre, B.; Hapiot, P.; Zuilhof, H. Tuning the Electronic Communication between Redox Centers Bound to Insulating Surfaces. *Angew. Chem., Int. Ed.* **2010**, *49*, 3157−3160.

(18) Hunger, R.; Fritsche, R.; Jaeckel, B.; Jaegermann, W.; Webb, L. J.; Lewis, N. S. Chemical and Electronic Characterization of Methyl-Terminated Si(111) Surfaces by High-Resolution Synchrotron Photoelectron Spectroscopy. *Phys. Rev. B* **2005**, *72*, 045317.

(19) Faucheux, A.; Gouget-Laemmel, A. C.; de Villeneuve, C. H.; Boukherroub, R.; Ozanam, F.; Allongue, P.; Chazalviel, J. N. Well-defined Carboxyl-terminated Alkyl Monolayers Grafted onto H-Si(111): Packing Density from a Combined AFM and Quantitative IR Study. *Langmuir* **2006**, *22*, 153−162.

(20) Maboudian, R.; Ashurst, W. R.; Carraro, C. Tribological Challenges in Micromechanical Systems. *Tribol. Lett.* **2002**, *12*, 95−100.

(21) Seitz, O.; Vilan, A.; Cohen, H.; Hwang, J.; Haeming, M.; Schoell, A.; Umbach, E.; Kahn, A.; Cahen, D. Doping Molecular Monolayers: Effects on Electrical Transport Through Alkyl Chains on Silicon. *Adv. Funct. Mater.* **2008**, *18*, 2102−2113.

(22) Böcking, T.; Kilian, K. A.; Gaus, K.; Gooding, J. J. Modifying Porous Silicon with Self-Assembled Monolayers for Biomedical Applications: The Influence of Surface Coverage on Stability and Biomolecule Coupling. *Adv. Funct. Mater.* **2008**, *18*, 3827−3833.

(23) Li, Y.; Calder, S.; Yaffe, O.; Cahen, D.; Haick, H.; Kronik, L.; Zuilhof, H. Hybrids of Organic Molecules and Flat, Oxide-Free Silicon: High-Density Monolayers, Electronic Properties, and Functionalization. *Langmuir* **2012**, *28*, 9920−9929.

(24) Faucheux, A.; Gouget-Laemmel, A. C.; Allongue, P.; de Villeneuve, C. H.; Ozanam, F.; Chazalviel, J. N. Mechanisms of Thermal Decomposition of Organic Monolayers Grafted on (111) Silicon. *Langmuir* **2007**, *23*, 1326−1332.

(25) Collins, G.; Kolesnik, M.; Krstic, V.; Holmes, J. D. Germanium Nanowire Synthesis from Fluorothiolate-Capped Gold Nanoparticles in Supercritical Carbon Dioxide. *Chem. Mater.* **2010**, *22*, 5235−5243.

(26) Mitsuya, M.; Sato, N. Energy Shift for Core Electron Levels of Chemisorbed Molecules Observed by X-ray Photoelectron Spectroscopy in the Course of Monolayer Growth on a Si(111) Surface. *Langmuir* **1999**, *15*, 2099−2102.

(27) Cheng, Y. A.; Zheng, B.; Chuang, P. H.; Hsieh, S. C. Solvent Effects on Molecular Packing and Tribological Properties of Octadecyltrichlorosilane Films on Silicon. *Langmuir* **2010**, *26*, 8256−8261.

(28) Colorado, R.; Lee, T. R. Wettabilities of Self-Assembled Monolayers on Gold Generated from Progressively Fluorinated Alkanethiols. *Langmuir* **2003**, *19*, 3288−3296.

(29) Mezger, M.; Sedlmeier, F.; Horinek, D.; Reichert, H.; Pontoni, D.; Dosch, H. On the Origin of the Hydrophobic Water Gap: An X-ray Reflectivity and MD Simulation Study. *J. Am. Chem. Soc.* **2010**, *132*, 6735−6741.

(30) Rodenstein, M.; Zurcher, S.; Tosatti, S. G. P.; Spencer, N. D. Fabricating Chemical Gradients on Oxide Surfaces by Means of Fluorinated, Catechol-Based, Self-Assembled Monolayers. *Langmuir* **2010**, *26*, 16211−16220.

(31) Tamada, K.; Ishida, T.; Knoll, W.; Fukushima, H.; Colorado, R.; Graupe, M.; Shmakova, O. E.; Lee, T. R. Molecular Packing of Semifluorinated Alkanethiol Self-assembled Monolayers on Gold: Influence of Alkyl Spacer Length. *Langmuir* **2001**, *17*, 1913−1921.

(32) te Riet, J.; Smit, T.; Coenen, M. J. J.; Gerritsen, J. W.; Cambi, A.; Elemans, J.; Speller, S.; Figdor, C. G. AFM Topography and Friction Studies of Hydrogen-Bonded Bilayers of Functionalized Alkanethiols. *Soft Matter* **2010**, *6*, 3450−3454.

(33) Ciampi, S.; Harper, J. B.; Gooding, J. J. Wet Chemical Routes to the Assembly of Organic Monolayers on Silicon Surfaces via the Formation of Si-C Bonds: Surface Preparation, Passivation and Functionalization. *Chem. Soc. Rev.* **2010**, *39*, 2158−2183.

(34) Gooding, J. J.; Ciampi, S. The Molecular Level Modification of Surfaces: From Self-Assembled Monolayers to Complex Molecular Assemblies. *Chem. Soc. Rev.* **2011**, *40*, 2704−2718.

(35) Rijksen, B.; Caipa Campos, M. A.; Paulusse, J. M. J.; Zuilhof, H. Silicon Radical Surface Chemistry. In *Encyclopedia of Radicals in Chemistry, Biology, and Materials*; Chatgilialoglu, C., Studer, A., Eds.; John Wiley & Sons: Chichester, West Sussex, U.K., 2012; p 2081.
(36) Buriak, J. M. Silicon-Carbon Bonds on Porous Silicon Surfaces. *Adv. Mater.* **1999**, *11*, 265−267.
(37) Buriak, J. M. Organometallic Chemistry on Silicon and Germanium Surfaces. *Chem. Rev.* **2002**, *102*, 1271−1308.
(38) Hurley, P. T.; Ribbe, A. E.; Buriak, J. M. Nanopatterning of Alkynes on Hydrogen-Terminated Silicon Surfaces by Scanning Probe-Induced Cathodic Electrografting. *J. Am. Chem. Soc.* **2003**, *125*, 11334−11339.
(39) de Smet, L.; Stork, G. A.; Hurenkamp, G. H. F.; Sun, Q. Y.; Topal, H.; Vronen, P. J. E.; Sieval, A. B.; Wright, A.; Visser, G. M.; Zuilhof, H.; Sudhölter, E. J. R. Covalently Attached Saccharides on Silicon Surfaces. *J. Am. Chem. Soc.* **2003**, *125*, 13916−13917.
(40) Sun, Q. Y.; de Smet, L.; van Lagen, B.; Giesbers, M.; Thune, P. C.; van Engelenburg, J.; de Wolf, F. A.; Zuilhof, H.; Sudhölter, E. J. R. Covalently Attached Monolayers on Crystalline Hydrogen-Terminated Silicon: Extremely Mild Attachment by Visible Light. *J. Am. Chem. Soc.* **2005**, *127*, 2514−2523.
(41) Sun, Q. Y.; de Smet, L.; van Lagen, B.; Wright, A.; Zuilhof, H.; Sudhölter, E. J. R. Covalently Attached Monolayers on Hydrogen Terminated Si(100): Extremely Mild Attachment by Visible Light. *Angew. Chem., Int. Ed.* **2004**, *43*, 1352−1355.
(42) Scheres, L.; Arafat, A.; Zuilhof, H. Self-Assembly of High-Quality Covalently Bound Organic Monolayers onto Silicon. *Langmuir* **2007**, *23*, 8343−8346.
(43) Scheres, L.; Rijksen, B.; Giesbers, M.; Zuilhof, H. Molecular Modeling of Alkyl and Alkenyl Monolayers on Hydrogen-Terminated Si(111). *Langmuir* **2011**, *27*, 972−980.
(44) Linford, M. R.; Fenter, P.; Eisenberger, P. M.; Chidsey, C. E. D. Alkyl Monolayers on Silicon Prepared from 1-Alkenes and Hydrogen-Terminated Silicon. *J. Am. Chem. Soc.* **1995**, *117*, 3145−3155.
(45) Sieval, A. B.; Linke, R.; Zuilhof, H.; Sudhölter, E. J. R. High-Quality Alkyl Monolayers on Silicon Surfaces. *Adv. Mater.* **2000**, *12*, 1457−1460.
(46) Rijksen, B.; van Lagen, B.; Zuilhof, H. Mimicking the Silicon Surface: Reactivity of Silyl Radical Cations toward Nucleophiles. *J. Am. Chem. Soc.* **2011**, *133*, 4998−5008.
(47) Allongue, P.; de Villeneuve, C. H.; Morin, S.; Boukherroub, R.; Wayner, D. D. M. The Preparation of Flat H-Si(111) Surfaces in 40% NH_4F Revisited. *Electrochem. Acta* **2000**, *45*, 4591−4598.
(48) Geer, R. E.; Stenger, D. A.; Chen, M. S.; Calvert, J. M.; Shashidhar, R.; Jeong, Y. H.; Pershan, P. S. X-ray and Ellipsometric Studies of Self-Assembled Monolayers of Fluorinated Chlorosilanes. *Langmuir* **1994**, *10*, 1171−1176.
(49) Banerjee, S.; Mulder, P.; Kleijn, J. M.; Cohen Stuart, M. A. Effect of Surface Roughness and Softness on Water Capillary Adhesion in Apolar Media. *J. Phys. Chem. A* **2012**, *116*, 6481−6488.
(50) Hutter, J. L.; Bechhoefer, J. Calibration of Atomic-Force Microscope Tips. *Rev. Sci. Instrum.* **1993**, *64*, 1868−1873.
(51) Stark, R. W.; Drobek, T.; Heckl, W. M. Thermomechanical Noise of a Free v-shaped Cantilever for Atomic-Force Microscopy. *Ultramicroscopy* **2001**, *86*, 207−215.
(52) Te Riet, J.; Smit, T.; Gerritsen, J. W.; Cambi, A.; Elemans, J.; Figdor, C. G.; Speller, S. Molecular Friction as a Tool to Identify Functionalized Alkanethiols. *Langmuir* **2010**, *26*, 6357−6366.
(53) Liu, W. H.; Bonin, K.; Guthold, M. Easy and Direct Method for Calibrating Atomic Force Microscopy Lateral Force Measurements. *Rev. Sci. Instrum.* **2007**, *78*, 063707.
(54) Rijksen, B.; Pujari, S. P.; Scheres, L.; van Rijn, C. J. M.; Baio, J. E.; Weidner, T.; Zuilhof, H. Hexadecadienyl Monolayers on Hydrogen-Terminated Si(111): Faster Monolayer Formation and Improved Surface Coverage Using the Enyne Moiety. *Langmuir* **2012**, *28*, 6577−6588.
(55) Frechette, J.; Maboudian, R.; Carraro, C. Thermal Behavior of Perfluoroalkylsiloxane Monolayers on the Oxidized Si(100) Surface. *Langmuir* **2006**, *22*, 2726−2730.
(56) van de Grampel, R. D.; Ming, W.; Gildenpfennig, A.; Laven, J.; Brongersma, H. H.; de With, G.; van der Linde, R. Quantification of Fluorine Density in the Outermost Atomic Layer. *Langmuir* **2004**, *20*, 145−149.
(57) Song, X. Y.; Zhai, J.; Wang, Y. L.; Jiang, L. Fabrication of Superhydrophobic Surfaces by Self-Assembly and Their Water-Adhesion Properties. *J. Phys. Chem. B* **2005**, *109*, 4048−4052.
(58) Bain, C. D.; Troughton, E. B.; Tao, Y. T.; Evall, J.; Whitesides, G. M.; Nuzzo, R. G. Formation of Monolayer Films by the Spontaneous Assembly of Organic Thiols from Solution onto Gold. *J. Am. Chem. Soc.* **1989**, *111*, 321−335.
(59) Folkers, J. P.; Laibinis, P. E.; Whitesides, G. M. Self-Assembled Monolayers of Alkanethiols on Gold: Comparisons of Monolayers Containing Mixtures of Short- and Long-chain Constituents with Methyl and Hydroxymethyl Terminal Groups. *Langmuir* **1992**, *8*, 1330−1341.
(60) Zisman, W, A., Relation of the Equilibrium Contact Angle to Liquid and Solid Constitution. In *Contact Angle, Wettability, and Adhesion*; American Chemical Society: Washington, D.C., 1964; Vol. *43*, pp 1−51.
(61) de Gennes, P. G. Wetting: Statics and Dynamics. *Rev. Mod. Phys.* **1985**, *57*, 827−863.
(62) Baier, R. E.; Shafrin, E. G.; Zisman, W. A. Adhesion: Mechanisms that Assist or Impede It. *Science* **1968**, *162*, 1360−1368.
(63) Nishino, T.; Meguro, M.; Nakamae, K.; Matsushita, M.; Ueda, Y. The Lowest Surface Free Energy Based on $-CF_3$ Alignment. *Langmuir* **1999**, *15*, 4321−4323.
(64) Ulman, A. Formation and Structure of Self-Assembled Monolayers. *Chem. Rev.* **1996**, *96*, 1533−1554.
(65) Schonherr, H.; Ringsdorf, H.; Jaschke, M.; Butt, H. J.; Bamberg, E.; Allinson, H.; Evans, S. D. Self-Assembled Monolayers of Symmetrical and Mixed Alkyl Fluoroalkyl Disulfides on Gold 0.2. Investigation of Thermal Stability and Phase Separation. *Langmuir* **1996**, *12*, 3898−3904.
(66) Kim, H. I.; Koini, T.; Lee, T. R.; Perry, S. S. Systematic Studies of the Frictional Properties of Fluorinated Monolayers with Atomic Force Microscopy: Comparison of CF_3- and CH_3-Terminated Films. *Langmuir* **1997**, *13*, 7192−7196.
(67) Yang, M.; Teeuwen, R. L. M.; Giesbers, M.; Baggerman, J.; Arafat, A.; de Wolf, F. A.; van Hest, J. C. M.; Zuilhof, H. One-Step Photochemical Attachment of NHS-Terminated Monolayers onto Silicon Surfaces and Subsequent Functionalization. *Langmuir* **2008**, *24*, 7931−7938.
(68) Hostetler, M. J.; Stokes, J. J.; Murray, R. W. Infrared Spectroscopy of Three-Dimensional Self-Assembled Monolayers: *N*-Alkanethiolate Monolayers on Gold Cluster Compounds. *Langmuir* **1996**, *12*, 3604−3612.
(69) Snyder, R. G.; Strauss, H. L.; Elliger, C. A. Carbon-Hydrogen Stretching Modes and the Structure of *n*-Alkyl Chains. 1. Long, Disordered Chains. *J. Phys. Chem.* **1982**, *86*, 5145−5150.
(70) Andersson, M. P.; Uvdal, P. New Scale Factors for Harmonic Vibrational Frequencies Using the B3LYP Density Functional Method with the Triple-ζ Basis Set 6-311+G(d,p). *J. Phys. Chem. A* **2005**, *109*, 2937−2941.
(71) Shaporenko, A.; Cyganik, P.; Buck, M.; Ulman, A.; Zharnikov, M. Self-Assembled Monolayers of Semifluorinated Alkaneselenolates on Noble Metal Substrates. *Langmuir* **2005**, *21*, 8204−8213.
(72) Sheparovych, R.; Motornov, M.; Minko, S. Low Adhesive Surfaces that Adapt to Changing Environments. *Adv. Mater.* **2009**, *21*, 1840−1844.
(73) Butt, H. J.; Kappl, M. Normal Capillary Forces. *Adv. Colloid Interface Sci.* **2009**, *146*, 48−60.
(74) Bhushan, B. *Handbook of Nanotechnology*, 2nd ed.; Springer-Verlag: New York, 2007; p 1222.
(75) Maugis, D. Adhesion of Spheres - The JRK-DMT Transition Using a Dugdale Model. *J. Colloid Interface Sci.* **1992**, *150*, 243−269.
(76) Shulha, H.; Kovalev, A.; Myshkin, N.; Tsukruk, V. V. Some Aspects of AFM Nanomechanical Probing of Surface Polymer Films. *Eur. Polym. J.* **2004**, *40*, 949−956.

(77) Lyklema, J. *Fundamentals of Interface and Colloid Science: Fundamentals*.; Academic Press: London, 1991; Vol. *1*.
(78) Urbakh, M.; Klafter, J.; Gourdon, D.; Israelachvill, J. The Nonlinear Nature of Friction. *Nature* **2004**, *430*, 525−528.
(79) Wu-Bavouzet, F.; Clain-Burckbuchler, J.; Buguin, A.; De Gennes, P. G.; Brochard-Wyart, F. Stick-Slip: Wet versus Dry. *J. Adhes.* **2007**, *83*, 761−784.
(80) Kim, H. I.; Boiadjiev, V.; Houston, J. E.; Zhu, X. Y.; Kiely, J. D. Tribological Properties of Self-Assembled Monolayers on Au, SiOx and Si Surfaces. *Tribol. Lett.* **2001**, *10*, 97−101.
(81) Houston, J. E.; Doelling, C. M.; Vanderlick, T. K.; Hu, Y.; Scoles, G.; Wenzl, I.; Lee, T. R. Comparative Study of the Adhesion, Friction, and Mechanical Properties of CF_3- and CH_3-Terminated Alkanethiol Monolayers. *Langmuir* **2005**, *21*, 3926−3932.
(82) Park, B.; Lorenz, C. D.; Chandross, M.; Stevens, M. J.; Grest, G. S.; Borodin, O. A. Frictional Dynamics of Fluorine-Terminated Alkanethiol Self-Assembled Monolayers. *Langmuir* **2004**, *20*, 10007−10014.